Environmental Pollution 273 (2021) 116421

Contents lists available at ScienceDirect

Environmental Pollution

journal homepage: www.elsevier.com/locate/envpol

Transboundary transport of ozone pollution to a US border region: A case study of Yuma☆

Zhen Qu [a, b, **], Dien Wu [c, 1], Daven K. Henze [a], Yi Li [d, 2, *], Mike Sonenberg [d], Feng Mao [d]

[a] Department of Mechanical Engineering, University of Colorado Boulder, Boulder, CO, 80309, USA
[b] School of Engineering and Applied Science, Harvard University, Cambridge, MA, 02138, USA
[c] Department of Atmospheric Sciences, University of Utah, Salt Lake City, UT, 84112, USA
[d] Arizona Department of Environmental Quality, Phoenix, AZ, 85007, USA

ARTICLE INFO

Article history:
Received 18 October 2020
Received in revised form
16 December 2020
Accepted 29 December 2020
Available online 4 January 2021

Keywords:
Ozone exceedances
Transboundary transport
GEOS-chem
Back trajectories

ABSTRACT

High concentrations of ground-level ozone affect human health, plants, and animals. Reducing ozone pollution in rural regions, where local emissions are already low, poses challenge. We use meteorological back-trajectories, air quality model sensitivity analysis, and satellite remote sensing data to investigate the ozone sources in Yuma, Arizona and find strong international influences from Northern Mexico on 12 out of 16 ozone exceedance days. We find that such exceedances could not be mitigated by reducing emissions in Arizona; complete removal of state emissions would reduce the maximum daily 8-h average (MDA8) ozone in Yuma by only 0.7% on exceeding days. In contrast, emissions in Mexico are estimated to contribute to 11% of the ozone during these exceedances, and their reduction would reduce MDA8 ozone in Yuma to below the standard. Using satellite-based remote sensing measurements, we find that emissions of nitrogen oxides (NO_x, a key photochemical precursor of ozone) increase slightly in Mexico from 2005 to 2016, opposite to decreases shown in the bottom-up inventory. In comparison, a decrease of NO_x emissions in the US and meteorological factors lead to an overall of summer mean and annual MDA8 ozone in Yuma (by ~1–4% and ~3%, respectively). Analysis of meteorological back-trajectories also shows similar transboundary transport of ozone at the US-Mexico border in California and New Mexico, where strong influences from Northern Mexico coincide with 11 out of 17 and 6 out of 8 ozone exceedances. 2020 is the final year of the U.S.-Mexico Border 2020 Program, which aimed to reduce pollution at border regions of the US and Mexico. Our results indicate the importance of sustaining a substantial cooperative program to improve air quality at the border area.

1. Introduction

Air pollution poses tremendous challenges to human health, ecosystems, and food security. Each year, about 4.2 million premature deaths are linked to ambient air pollution globally (Cohen et al., 2017). Among these, long-term ozone (O_3) exposure is estimated to cause 1.04–1.23 million respiratory deaths in adults (Malley et al., 2017) owing to respiratory mortality (Jerrett et al., 2009) e.g., chronic obstructive pulmonary disease (COPD) (Zanobetti and Schwartz, 2011). Short-term exposure to ozone has demonstrated associations with asthma, acute respiratory infections, pneumonia, COPD, upper respiratory tract inflammation, and increased mortality for those with prior admission for acute myocardial infarction (Medina-Ramon et al., 2006; Zanobetti and Schwartz 2006; Malig et al., 2016; Bero Bedada et al., 2016).

To combat ozone pollution, the Clean Air Act (CAA) requires the United States Environmental Protection Agency (US EPA) to set National Ambient Air Quality Standards (NAAQS) for pollutants considered harmful to public health and the environment. The primary standard for ozone (evaluated using design value, which is the 3-year average of the annual 4th highest daily maximum 8-h average ozone concentration) was recently revised from the 2008 standard of 75 parts per billion by volume (ppbv) to 70 ppbv in

☆ This paper has been recommended for acceptance by Pavlos Kassomenos.

* Corresponding author.
** Corresponding author. Department of Mechanical Engineering, University of Colorado Boulder, Boulder, CO, 80309, USA.
E-mail addresses: zhen.qu@colorado.edu (Z. Qu), lyggd0910@gmail.com (Y. Li).
[1] Now at: Division of Geological and Planetary Sciences, California Institute of Technology, Pasadena, CA,91125, USA.
[2] Now at: Sailbri Cooper Inc., Tigard, OR, 97223, USA.

https://doi.org/10.1016/j.envpol.2020.116421

October 2015, leading to 25 new nonattainment areas (Table S1). In general, nonattainment areas are located in or near metropolitan counties, have intensive local industrial activities (Schnell et al., 2016), or are affected by wintertime shallow boundary inversions (Schnell et al., 2009) and sea breeze (G rossi et al., 2004; Stauffer et al., 2015). However, there are a few exceptional non-attainment rural regions at the international borders.

The new ozone standard can be extremely challenging to attain for rural border regions such as Yuma County in Arizona, Imperial County in California, and Doña Ana County in New Mexico. Compared to urban ozone non-attainment regions (e.g., Maricopa County in the Phoenix metropolitan area), these three counties have much lower population, emissions, and emissions-related activities but comparable elevated ozone concentrations (see Table S2). These counties are all located near the international US-Mexico border and thus impacted by both domestic and international emissions. For example, Yuma has 95% less population, 87% (NO_x) and 91% (volatile organic compounds (VOCs)) less emissions of ozone precursors, and 95% less vehicle miles travelled (VMT) than Maricopa. Nonetheless, Yuma has an ozone design value of 74 ppbv, close to the 77 ppbv value for Phoenix. Although ozone design values in Yuma have decreased from 2014 to 2018 (Figure S1), Yuma faces additional challenges of international and interstate transport of ozone and its precursors due to its geographical location, since Yuma is bordered by California on the west and Mexico on the south and the southwest.

Previous studies have demonstrated that the trans-boundary transport of Asian pollution contributes to enhancement of background ozone in the western US (Goldstein et al., 2004; Zhang et al., 2008; Zhang et al., 2014; Fiore et al., 2014; Verstraeten et al., 2015; Jaffe et al., 2018) and the transport of aerosols from Canada and Mexico to the US (Park et al., 2006). Here, we show that the air pollutants in Mexico also have significant contributions to the elevated ozone concentration in the US border counties like Yuma. We explicitly trace sources of ozone in Yuma using back trajectories. Locations where emission reductions can lead to the largest decrease of MDA8 ozone on exceedance days are evaluated using receptor-oriented chemical transport modelling (Cacuci, 1981a, 1981b; Marchuk, 1995; Marchuk et al., 1996; Fisher and Lary 1995; Sandu et al., 2005; Hakami et al., 2006; Zhang et al., 2009). We also separately evaluate the impact of NO_x and VOC concentrations and meteorological factors on long-term ozone trends in Yuma.

2. Methods

2.1. Surface measurement and meteorology data

We used surface measurements of ozone concentration at the Yuma Supersite from the EPA Air Quality System (AQS) (AQS ID: 04-027-8011). The Yuma Supersite is located in the southwestern portion of Yuma County. The first valid ozone design value from the Yuma Supersite monitor starts in 2010 (for the years 2010 2012). Wind speed and wind directions at the Yuma International Airport (4 km south of Yuma Supersite) are used to study the correlation between ozone exceedances and transport from outside Yuma. Timeseries of temperature are from the GEOS-FP assimilated meteorological reanalysis fields at the $0.25^\circ \times 0.3125^\circ$ resolution.

2.2. STILT back trajectories

The Stochastic Time-Inverted Lagrangian Transport (STILT) model (Lin et al., 2003; Fasoli et al., 2018) was used to perform back-trajectory and footprint analyses for Yuma County (Yuma Supersite, 32.69°N, 114.61°W), Imperial County (Calexico-Ethel Street, 32.68°N, 115.48°W), and Dona Ana County (Desert View, 31.80°N, 106.58°W). STILT is a Lagrangian particle dispersion model. It employs a mean advection scheme from the Hybrid Single−Particle Lagrangian Integrated Trajectory (HYSPLIT) system (Draxler and Hess, 1998), but implements a different turbulent module. STILT is typically applied to track upwind air parcels to represent airflows and reveal surface influences on downwind location. Previous studies have used STILT to evaluate the impact of interactions among different layers of the atmosphere on surface ozone concentrations (de Fatima et al., 2012) and sources of ozone at low altitudes from different vertical layers (Ryoo et al., 2017).

Air parcels in STILT were driven by the High-Resolution Rapid Refresh (HRRR) meteorological field (Rolph et al., 2017). At each site, 500 air parcels are released per hour during the 8 h that have the highest ozone concentrations and dispersed back in time for 24 h. The model tracks the trajectories backward in time for each receptor. Each daily back trajectory is the average of all 800 particles released in that day. The receptor height was set as 5 m above the surface to match the general height of the ground-based monitoring equipment. The daily mean back trajectory is calculated based on the average locations of all 4000 trajectories of that day.

The STILT footprint was calculated at the 0.01° resolution on exceeding days to infer all possible source regions. This footprint describes the sensitivity of changes in concentration at the monitoring site to upstream surface fluxes. It is calculated by summing up all the sensitivities of air parcels within a grid volume from the surface to the mixed layer height. Therefore, the stronger the air parcels interact with the surface (e.g., more particles concentrated below the PBL), the higher the footprint values are.

2.3. GEOS-chem and its adjoint

GEOS-Chem is a 3D chemical transport model (CTM) driven by assimilated meteorology data from the National Aeronautics and Space Administration (NASA) Global Modelling and Assimilation Office (GMAO). We employed the Modern-Era Retrospective analysis for Research and Applications, Version 2 (MERRA-2) meteorological field for global $2^\circ \times 2.5^\circ$ simulation from 2005 to 2017, and used the Goddard Earth Observing System (GEOS-5) meteorological field at the native $0.5^\circ \times 0.667^\circ$ resolution for the nested North America simulations. Both simulations use 47 vertical layers. GEOS-Chem includes a detailed ozone-NO_x-hydrocarbon chemical mechanism (Bey et al., 2001), partitioning of NO_x/HNO_3 (Park et al., 2004), and uptake of NO_2, NO_3, and N_2O_5 on aerosol (Martin et al., 2003; Evans and Jacob, 2005). The hydrocarbon mechanism includes ethane, propane, isoprene, acetone, acetaldehyde, methyl ethyl ketone, $\geq$ C3 alkenes, and $\geq$ C4 alkanes. We use anthropogenic emissions of NO_x, sulfur dioxide (SO_2), ammonia (NH_3), carbon monoxide (CO), non-methane VOCs (NMVOCs) and primary aerosol from the HTAP 2010 inventory version 2 (Janssens-Maenhout et al., 2015). Three hourly biomass burning emissions are from the Global Fire Emissions Database version 4 (GFEDv4) (Giglio et al., 2013). We replaced bottom-up NO_x emissions with global top-down estimates (Qu et al., 2017, 2020) for NO_2 and ozone trend simulations.

The GEOS-Chem adjoint model v35f (Henze et al., 2007) is used for source apportionment calculations. It is based on version 8-2-03 of GEOS-Chem, with bug fixes and updates up to version 10. It includes the adjoint for model processes of aerosol thermodynamics, chemistry, convection, turbulent mixing, advection, and wet removal. This model provides an efficient way to calculate the sensitivity of model variables (e.g., simulated surface MDA8 ozone concentrations in the grid cell that includes Yuma during the exceedance days) to model parameters (e.g., NO_x and isoprene

emissions) (Zhang et al., 2015; Walker et al., 2012; Lapina et al., 2014, 2015).

2.4. OMI NO_2 and HCHO observations

We used NO_2 and formaldehyde (HCHO) column densities from the Ozone Monitoring Instrument (OMI) to study the trend of NO_2 and VOC concentrations in the US and Mexico. Oxidation of highly reactive VOCs produce HCHO near the emission sources. HCHO can be observed by satellite and used to track the trend of VOC concentrations (Stavrakou et al., 2009; Zhu et al., 2017; Shen et al., 2019). Global top-down NO_x emissions from 2005 to 2016 are derived at the $2^\circ \times 2.5^\circ$ resolution using the OMI NO_2 observations following the method of Qu et al., (2017), as reported in Qu et al., (2020). OMI is a UV/Visible nadir solar backscatter spectrometer aboard the National Aeronautics and Space Administration (NASA) Aura satellite with a local overpass time of about 13:45. It was launched in 2004 and has a nadir resolution of 13 km $\times$ 24 km. Three OMI NO_2 Level 2 retrieval products, the $OMNO_2$ version 3 of NASA standard product (NASA SP) (Krotkov et al., 2017), the Dutch OMI NO_2 (DOMINO) version 2 from KNMI (Boersma et al., 2011) and the BErkeley High-Resolution (BEHR) version 2.1c from UC Berkeley (Russell et al., 2011) are used to analyze trends of NO_2 vertical column densities. The NASA and the DOMINO products are also applied to derive global top-down NO_x emissions. We employed the OMI HCHO Level 2 product version 3 OMHCHO from NASA (https://disc.gsfc.nasa.gov/datasets/OMHCHO_V003/summary?keywords=OMHCHO) to study the trend of biogenic non-methane VOC column concentrations. We only included retrievals that have cloud fractions between 0 and 0.5, excluded data affected by row anomalies (http://projects.knmi.nl/omi/research/product/rowanomaly-background.php), and filtered the data using data quality flags.

3. Results and discussion

3.1. Impact of transport on ozone exceedance in yuma

The peak of MDA8 ozone and most exceedances in Yuma happen in May and June (Fig. 1). Temperature is typically a dominant factor that affects the ozone peak due to local ozone formation (Atkinson, 1990; Vukovich and Sherwell, 2003; Wise, 2009; Stathopoulou et al., 2008). In Yuma, however, the peak of surface temperature and ozone concentrations are not aligned; the surface temperature peaks during the monsoon season in July and August (Figure S1), following the peak of ozone concentrations in May and June. Yuma has a desert climate with less than three days per month of rainfall, so we do not expect variations in precipitation affect ozone formation in Yuma. We also rule out the impact of temperature inversions on ozone exceedances in Figure S2. In fact, changes in horizontal and vertical transport (e.g., stratospheric intrusion) are more important to ozone exceedances in locations like Yuma, where ozone originates mostly from non-local sources. The winds in Yuma are mostly from the southwest during the high ozone months (Figure S3) and switch towards emanating from the south and the southeast when the temperature peaks (Adams and Comrie, 1997). More specifically, during the hours that ozone concentrations in Yuma were higher than 70 ppbv from 2010 to 2016 (Fig. 2(a)), wind directions were from the southwest 71% of the time and from the west 11% of the time. These correlations between wind direction and high ozone events suggest transport from the international border on the southwest.

Longer distance ozone transport to Yuma are investigated using daily mean back-trajectory calculations through STILT. In Fig. 2(b), a majority of ozone exceedances in Yuma coincide with back-trajectories over California and Mexico. In the summer (see Figure S4), most back-trajectories are from the south and the west, suggesting the impact of precursor gases in northern Mexico and southern California on ozone concentrations in Yuma. In the spring and fall, about half of the trajectories come from the north, but trajectories during the ozone exceedance days are from southern California and northern Mexico. Footprint analysis further show that Northern Mexico takes up ~75% of the regions that have strong surface influences on pollution in Yuma (footprint $> 10^{-4}$ ppm μmol^{-1} m^2 s, see Figure S4(a)). The limitation of these analyses is that the impact of chemical formation and decay on ozone are not included. They only show how ozone already formed in other regions transports to Yuma from upwind regions.

3.2. Sensitivities of peak afternoon ozone in Yuma to emissions

We use GEOS-Chem adjoint model to further identify locations where ozone precursor gas emissions have the largest contribution to ozone concentrations in Yuma. The timeseries of simulated MDA8 ozone using this model and bottom-up emissions capture the higher magnitude in May and June but have smaller seasonal variations than the measurements ($R^2 = 0.5$, see Figure S6). The simulation captures some of the ozone exceedance and most day-to-day variations in Yuma (NMSE = 0.04). However, the simulations have a slightly bias high (NMB = 5%) compared to the measurements from March to October of 2014 and have limitations in

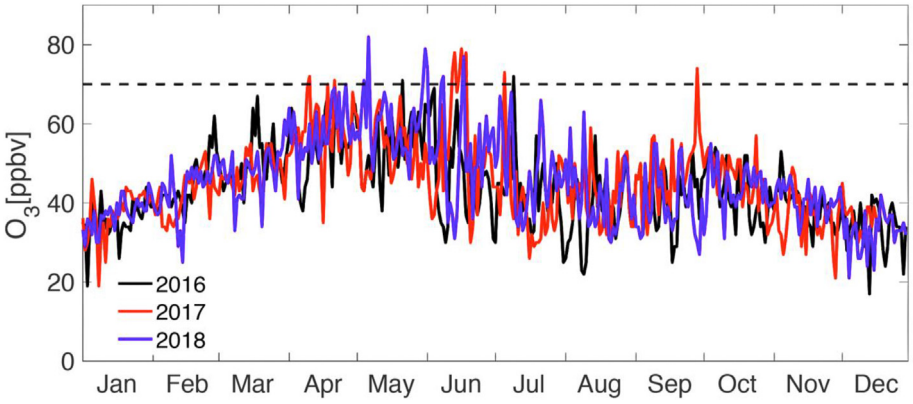

Fig. 1. Timeseries of MDA8 ozone at the Yuma Supersite in 2016 (black), 2017 (red) and 2018 (blue). (For interpretation of the references to colour in this figure legend, the reader is referred to the Web version of this article.)

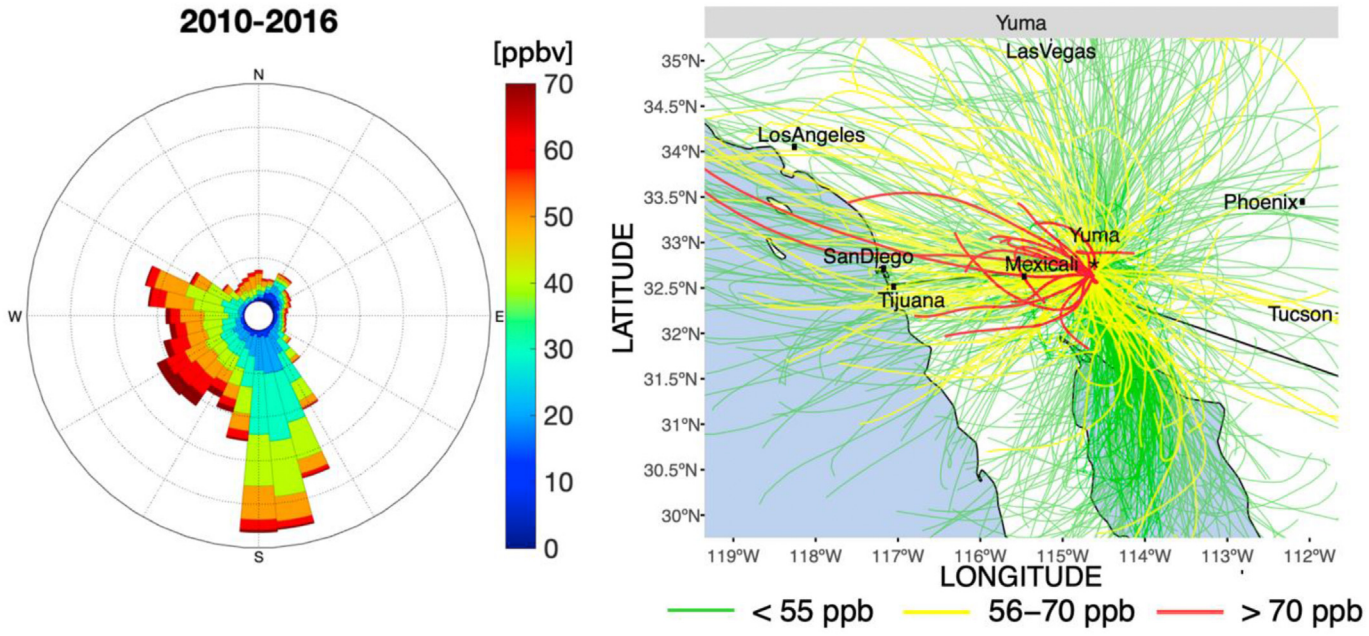

Fig. 2. (a) Wind directions and ozone concentrations in Yuma from April to July of the year 2010–2016. The length of each "spoke" represents the frequency of wind blew from that direction. (b) STILT 24 h back trajectories for Yuma in 2016–2018. Each line represents a daily mean trajectory of 4000 particles released 5 m above the surface during the 8 h that have the maximum ozone concentrations of the day. Back trajectories in red represent days when MDA8 exceed the EPA standard of 70 ppbv; trajectories in yellow represent days when air quality is acceptable; trajectories in green represent days when air quality is good. (For interpretation of the references to colour in this figure legend, the reader is referred to the Web version of this article.)

capturing the inter-annual variations of measured MDA8 ozone (see Table S3).

To perform source attribution, we define a model receptor metric to be the simulated MDA8 surface ozone concentration in Yuma on the exceedance days (see Table S5) between June 11th and July 1st in 2010. The adjoint model calculates the sensitivity of this metric with respect to emission scaling factors of each species, sector, and model grid cell over these 50 days. The simulation starts on May 11th and ends on July 2nd. Since the wind and ozone patterns are similar in all years from 2010 to 2016 (except for 2011, see Fig. S7), sensitivity analysis in 2010, consistent with the year of the HTAP emission inventory, is taken to be representative of the impact of emissions on ozone concentrations in Yuma.

Fig. 3 shows the largest sensitivities of MDA8 ozone in Yuma to precursor emissions mainly lie in California and Mexico. Each pixel represents the first order response of surface ozone concentrations in Yuma to a change in (a) anthropogenic NO_x (including emissions from aircraft, ships, energy, industry, transportation, residential, and agriculture) and (b) biogenic isoprene emissions in the corresponding grid cell. Assuming a linear ozone response, removing all anthropogenic NO_x (isoprene) emissions in Mexico, California and Arizona would lead to a decrease of 2.5 ppbv (0.2 ppbv), 1.7 ppbv (1.3 ppbv) and 0.2 ppbv (0.006 ppbv) decrease of MDA8 ozone in Yuma. Removing anthropogenic and natural sources of all species in Mexico and California would reduce MDA8 ozone during the exceedance days by 5.5 ppbv (11% of total MDA8 ozone in Yuma) and 3.8 ppbv (8%), respectively, which are sufficient to attain the ozone standard in Yuma. In comparison, removing all emissions in Arizona would only reduce this value by 0.4 ppbv (0.7%), which would insufficient for Yuma to attain the ozone NAAQS. Biogenic VOC emissions from the ocean are not included in the model. However, given the footprint analysis in Figure S5, we do not expect much contribution from ocean sources.

3.3. Long-term trends of ozone and its precursors

As shown in Fig. 4(a), the annual mean MDA8 ozone and summertime 24-h mean surface ozone from measurements have been decreasing in Yuma from 2010 to 2018; the number of ozone exceedance days has fluctuated despite a downward trend. However, ozone precursor gases have mixed trends. For instance, the trend of non-methane VOCs, approximated by the trend of formaldehyde concentration from the OMI observations (Palmer et al., 2003, 2006; Millet et al., 2008), show increases of 41% in northern Mexico, 33% in Arizona, and 43% in southern California from 2005 to 2017, mainly due to changes in temperature as explained by Zhu et al., (2017). OMI NO_2 column concentrations show no significant trend in Arizona, decrease by 21% (DOMINO retrieval) – 32% (NASA retrieval) in southern California, and increase by 2% (NASA retrieval) – 25% (DOMINO retrieval) in northern Mexico from 2005 to 2017 (see Figure S8 and S9). These trends suggest increasing contributions to the Yuma ozone from NO_2 in northern Mexico and biogenic non-methane VOCs in all studied regions. However, decreases in NO_2 concentrations in California are likely counteracting the increases.

To quantify contributions of NO_x to ozone concentration in Yuma, we estimate top-down NO_x emissions using the NASA retrieval and the DOMINO retrieval following Qu et al., (2017, 2020). As shown in Qu et al., (2020), top-down NO_x emissions decrease by 20% (constrained by the NASA product) – 26% (constrained by the DOMINO product) in the US from 2006 to 2015. In comparison, top-down NO_x emissions in Mexico have increased by 12% (NASA) – 13% (DOMINO) from 2006 to 2015. This is in contrast to the decreasing trend in NO_x emissions in Mexico in the EPA National Emission Inventory (NEI). According to NEI, the total anthropogenic NO_x emissions in Mexico have reduced by 11% from 2008 (0.82 TgN) to 2017 (0.73 TgN), with an annual budget of 0.76 TgN in 2011 and 0.79 TgN in 2014, but this trend is likely subject to large uncertainties. The base year emissions in 2008 are from Inventario

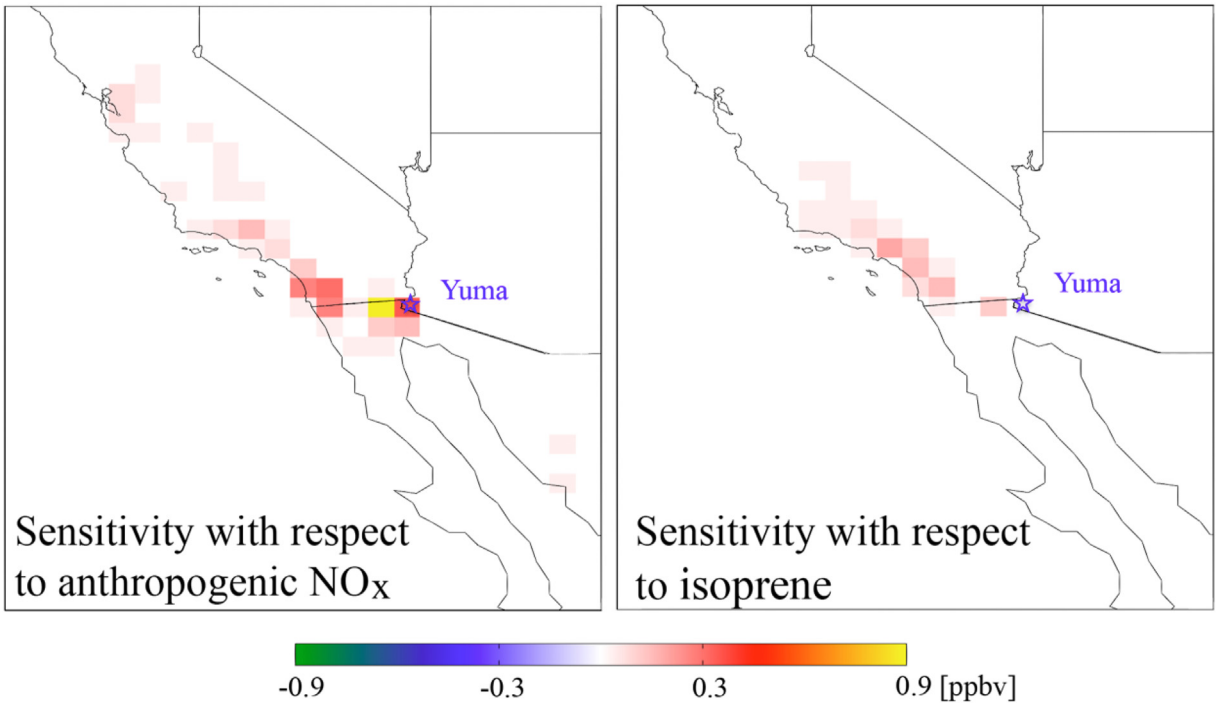

Fig. 3. Sensitivity of simulated MDA8 ozone in Yuma on the exceedance days (between June 11th and July 1st in 2010, based on Air Quality System (AQS) measurements) to fractional changes in (a) anthropogenic NO_x and (b) biogenic isoprene emissions from May 11th to July 1st. The stars mark the grid cell that includes Yuma.

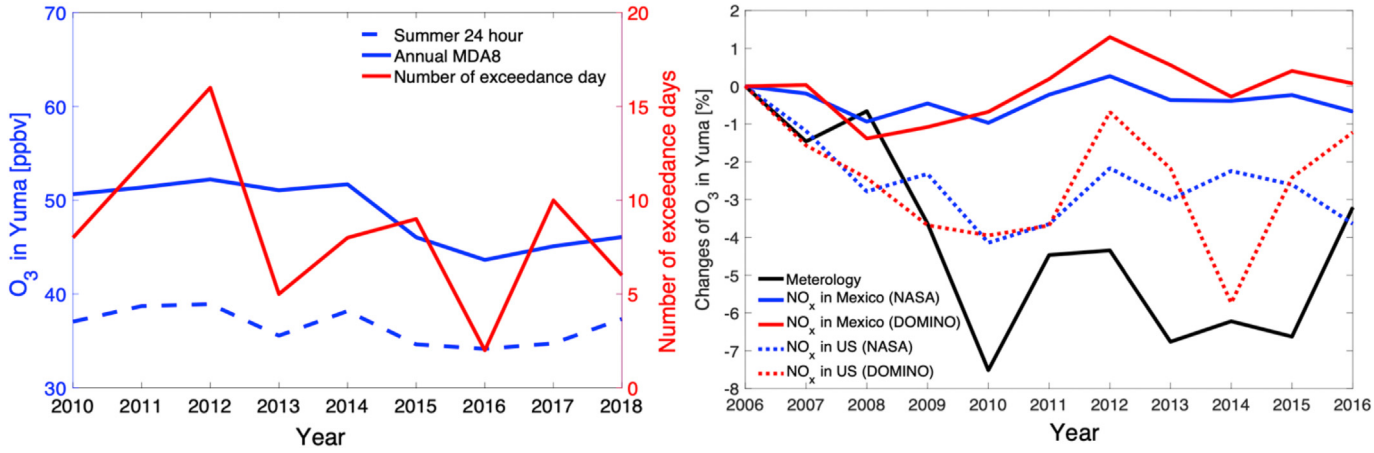

Fig. 4. (A) Annual MDA8 (solid line) and summer 24 h mean (dashed line) ozone (blue) and number of ozone exceedance days (red) at the Yuma Supersite from 2010 to 2018; (b) Changes of summertime ozone (24-h average) in Yuma due to changes in NO_x emissions (DOMINO posterior shown in red, NASA posterior shown in blue) and meteorology (black), the latter based on a simulation using the same anthropogenic emissions in all years. (For interpretation of the references to colour in this figure legend, the reader is referred to the Web version of this article.)

Nacional de Emissions de Mexico. EPA projected anthropogenic NO_x emissions in 2014 based on 2008 data, and linearly interpolated 2011 emissions between 2008 and projected 2014 emissions. Projected emissions in 2018 from the Eastern Research Group are directly used for 2017. These projections have large uncertainties and may not reflect the growing contribution of NO_x emissions from industrial, areal, and off-road mobile sources, as well as the slower than expected decreases in on-road diesel NO_x emissions as previously reported for the United States (Jiang et al., 2018). The discrepancy between the top-down and bottom-up estimates may also reflect the increasing contribution from background NO_2 if GEOS-Chem simulation cannot accurately represent it as shown in Silvern et al., (2019).

The GEOS-Chem simulation has a similar decreasing trend of summertime ozone in Yuma as the surface measurements. We therefore use GEOS-Chem to separate the contribution of NO_x emissions from the US and Mexico to the summertime ozone trend in Yuma. Fig. 4(b) shows the simulated changes of surface ozone in Yuma due to emission changes in different regions. This trend is mainly impacted by meteorology (black line, leading to a 3% decrease) and the decrease of NO_x emissions in the US (dotted lines in Fig. 4(b), contributing to 1–4% decrease from 2006 to 2015). The changes of NO_x emissions in Mexico (red and blue solid lines in Fig. 4(b)) barely impact the ozone trend in Yuma (by less than 1%). Simulated MDA8 ozone in Yuma has smaller variations than the summertime means ozone (Figure S10) – meteorology and NO_x

emissions in Mexico and the US each lead to less than 2% changes from 2006 to 2015.

4. Policy implications

We investigated the sources of ozone in Yuma, a new non-attainment area due to stricter ozone NAAQS, using ground-based measurement data, back trajectories and footprints, adjoint sensitivity analysis, satellite observations, and chemical transport modelling. Transported pollution from Mexico has the largest contribution to surface ozone in Yuma from adjacent regions (Arizona, California, and Mexico). However, unlike the decreasing trend of NO_x emissions in Mexico as shown in EPA NEI, top-down estimates show increases of NO_x emission in Mexico, which have increasing contributions relative to those from the US to the summertime ozone in Yuma. These differences in top-down and bottom-up NO_x emissions call for more accurate pollutant source estimates in Mexico and better understanding of background NO_2 concentrations, especially considering their relatively increasing importance as anthropogenic emissions in the US decline. In addition to anthropogenic sources, biogenic isoprene from California (e.g., Geron et al., 2006; Fares et al., 2011; Misztal et al., 2014) also contribute to 1.3 ppbv of ozone in Yuma on exceedance days in 2010.

The Clean Air Act requires that moderate and above non-attainment areas must have plans for meeting a 15% reduction of VOC (or NO_x, when specific conditions apply) emissions within 6 years of designation. These could impede development of new industries, limit employment, and hurt local economies with little improvement to air quality for rural areas like Yuma, where local emissions are already low. According to the sensitivity tests, eliminating all local sources of emissions in Arizona only leads to 0.7% (0.4 ppbv) reduction of MDA8 ozone on exceedance days, which is not sufficient to bring ozone concentrations in Yuma into attainment with federal standards. Although the state can seek to exclude ozone exceedances from the data record by showing they were caused by an exceptional event (e.g., stratospheric intrusion, wildfire, transport of ozone from upwind areas, trapped precursors by strong inversions), or avoid more stringent federal requirements by showing the exceedances are due to international transport and not to domestic emissions, the fact remains that the environmental and health issues of residents in these non-attainment regions cannot be improved without reducing emissions from upwind states and countries.

Several other ozone non-attainment regions located along the US-Mexico border are also affected by international pollution transport. For instance, daily mean back-trajectories from Dona Ana County of New Mexico and Imperial County of California (Fig. S11) show that 16% and 50% of the ozone exceedances are transported from Northern Mexico. Footprint analysis also shows that Northern Mexico contribute to strong surface influence (footprint $> 10^{-4}$ ppm μmol^{-1} m^2 s) on ~11 out of 17 and ~6 out of 8 exceedances in Dona Ana and Imperial in 2018 (Fig. S4). There are several Electric Generating Units (EGU) in Mexico located along the border with the US according to Mexico's Ministry of Energy, which are large sources of ozone precursor gases to border counties. However, unlike Yuma, ozone exceedances at these two locations can also benefit from emission reductions inside the state.

Canada and the US reached a Canada-U.S. Air Quality Agreement in 1991 to address transboundary air pollution and added an ozone annex with specific emission control measures of NO_x and VOCs in the border region in 2000. Consequently, NO_x, VOCs, and ozone concentrations within 500 km of the US-Canada Border have decreased from 1995 to 2014 (EPA, 2016). U. S. and Mexico are collaborating through the Border 2020 Program to reduce air pollution in the border region. However, our results show that the current air pollution control in Mexico barely helps reduce ozone concentrations in Yuma. More effective interstate partnership and international agreement between the US and Mexico to reduce sources of NO_x and VOCs as well as ozone and particulate matter exceedances would yield a variety of positive benefits on human health and ecosystems for the downwind regions.

Author statement

Zhen Qu: Conceptualization, Investigation, Software, Validation, Writing – original draft, Supervision. Dien Wu: Methodology, Investigation, Validation, Software. Daven K. Henze: Conceptualization, Writing - original draft. Yi Li: Conceptualization, Investigation, Writing – original draft, Supervision. Mike Sonenberg: Investigation, Data curation, Writing – review & editing. Feng Mao: Data curation, Software, Methodology

Declaration of competing interest

The authors declare that they have no known competing financial interests or personal relationships that could have appeared to influence the work reported in this paper. The authors confirm that there are no conflicts of interest.

Acknowledgements

Z. Qu and D. K. Henze acknowledge funding support from National Aeronautics and Space Administration (NASA) HAQAST NNX16AQ26G. Z. Qu would like to acknowledge high-performance computing support from Cheyenne (doi:10.5065/D6RX99HX) provided by NCAR's Computational and Information Systems Laboratory, sponsored by the National Science Foundation. D. Wu would like to acknowledge the support and resources from the Center for High Performance Computing (CHPC) at the University of Utah. The authors thank the Air Quality Monitoring and Assessments section of Arizona Department of Environmental Quality for assistance with the surface monitoring data.

Appendix A. Supplementary data

Supplementary data to this article can be found online at https://doi.org/10.1016/j.envpol.2020.116421.

References

Adams, D.K., Comrie, A.C., 1997. The north American monsoon. Bull. Am. Meteorol. Soc. 78 (10), 2197–2214. https://doi.org/10.1175/1520-0477(1997)078<2197:TNAM>2.0.CO;2.

Atkinson, R., 1990. Gas-phase tropospheric chemistry of organic compounds: a review. Atmos. Environ. 24 (1), 1–41. https://doi.org/10.1016/j.atmosenv.2007.10.068.

Bero Bedada, G., Raza, A., Forsberg, B., Lind, T., Ljungman, P., Pershagen, G., Bellander, T., 2016. Short-term exposure to ozone and mortality in subjects with and without previous cardiovascular disease. Epidemiology 27 (5). https://doi.org/10.1097/EDE.0000000000000052.

Bey, I., Jacob, D.J., Yantosca, R.M., Logan, J.A., Field, B.D., Fiore, A.M., Li, Q., Liu, H.Y., Mickley, L.J., Schultz, M.G., 2001. Global modeling of tropospheric chemistry with assimilated meteorology: model description and evaluation. J. Geophys. Res. Atmos. 106 (D19), 23073–23095. https://doi.org/10.1029/2001JD000807.

Boersma, K.F., et al., 2011. An improved tropospheric NO_2 column retrieval algorithm for the Ozone Monitoring Instrument. Atmos. Meas. Tech. 4 (9), 1905–1928. https://doi.org/10.5194/amt-4-1905-2011.

Cacuci, D.G., 1981a. Sensitivity theory for nonlinear systems. I. Nonlinear functional analysis approach. J. Math. Phys. 22 (12), 2794–2802. https://doi.org/10.1063/1.525186.

Cacuci, D.G., 1981b. Sensitivity theory for nonlinear systems. II. Extensions to additional classes of responses. J. Math. Phys. 22 (12), 2803–2812. https://doi.org/10.1063/1.524870.

Cohen, et al., 2017. Estimates and 25-year trends of the global burden of disease

attributable to ambient air pollution: an analysis of data from the Global Burden of Disease Study. Lancet 389, 1907–1918. https://doi.org/10.1016/S0140-6736(17)30505-6.
de Fátima, A.M., et al., 2012. Ozone sounding in the metropolitan area of são paulo, Brazil: wet and dry season campaigns of 2006, *atmos*. Environ. Times 61, 627–640. https://doi.org/10.1016/j.atmosenv.2012.07.083.
Draxler, R., Hess, G., 1998. An overview of the HYSPLIT_4 modelling system for trajectories. Aust. Meteorol. Mag. 47 (4), 295–308.
EPA, 2016. Canada-United States air quality agreement progress Report 2016. https://www.epa.gov/sites/production/files/2018-02/documents/5129_canada-united_states_air_quality_agreement_progress_report_2016_en05.pdf.
Evans, M.J., Jacob, D.J., 2005. Impact of new laboratory studies of N2O5 hydrolysis on global model budgets of tropospheric nitrogen oxides, ozone, and OH. Geophys. Res. Lett. 32 (9), L09813. https://doi.org/10.1029/2005GL022469.
Fares, S., Gentner, D.R., Park, J., Ormeno, E., Karlik, J., Goldstein, A.H., 2011. Biogenic emissions from Citrus species in California. Atmos. Environ. 45, 4557–4568. https://doi.org/10.1016/j.atmosenv.2011.05.066.
Fasoli, B., Lin, J.C., Bowling, D.R., Mitchell, L., Mendoza, D., 2018. Simulating atmospheric tracer concentrations for spatially distributed receptors: updates to the Stochastic Time-Inverted Lagrangian Transport model's R interface (STILT-R version 2). Geosci. Model Dev. 11 (7), 2813–2824. https://doi.org/10.5194/gmd-11-2813-2018.
Fiore, A.M., Oberman, J.T., Lin, M.Y., Zhang, L., Clifton, O.E., Jacob, D.J., Naik, V., Horowitz, L.W., Pinto, J.P., Milly, G.P., 2014. Estimating North American background ozone in U.S. surface air with two independent global models: variability, uncertainties, and recommendations. Atmos. Environ. 96, 284–300. https://doi.org/10.1016/j.atmosenv.2014.07.045.
Fisher, M., Lary, D.J., 1995. Lagrangian four-dimensional variational data assimilation of chemical species. Q. J. Roy. Meteorol. Soc. 121 (527), 1681–1704. https://doi.org/10.1002/qj.49712152709.
Geron, C., Guenther, A., Greenberg, J., Karl, T., Rasmussen, R., 2006. Biogenic volatile organic compound emissions from desert vegetation of the southwestern US. Atmos. Environ. 40, 1645–1660. https://doi.org/10.1016/j.atmosenv.2005.11.011.
Giglio, L., Randerson, J.T., Werf, G.R., 2013. Analysis of daily, monthly, and annual burned area using the fourth-generation global fire emissions database (GFED4). J. Geophys. Res. Biogeosci. 118 (1), 317–328. https://doi.org/10.1002/jgrg.20042.
Goldstein, A.H., Millet, D.B., McKay, M., Jaegle, L., Horowitz, L., Cooper, O., Hudman, R., Jacob, D.J., Oltmans, S., Clarke, A., 2004. Impact of asian emissions on observations at trinidad head, California, during ITCT 2K2. J. Geophys. Res. Atmos. 109 (D23) https://doi.org/10.1029/2003JD004406.
G rossi, P., Thunis, P., Martilli, A., Clappier, A., 2004. Effect of sea breeze on air pollution in the greater Athens area: analysis of different emission scenarios. J. Appl. Meteorol. 563–575. https://doi.org/10.1175/1520-0450(2000)039<0563:EOSBOA>2.0.CO;2.
Hakami, A., Seinfeld, J.H., Chai, T., Tang, Y., Carmichael, G.R., Sandu, A., 2006. Adjoint sensitivity analysis of ozone nonattainment over the continental United States. Environ. Sci. Technol. 40 (12), 3855–3864. https://doi.org/10.1021/es052135g.
Henze, D.K., Hakami, A., Seinfeld, J.H., 2007. Development of the adjoint of GEOS-Chem. Atmos. Chem. Phys. 7 (9), 2413–2433. https://doi.org/10.5194/acp-7-2413-2007.
Jaffe, D.A., Cooper, O.R., Fiore, A.M., Henderson, B.H., Tonneson, G.S., Russell, A.G., Henze, D.K., Langford, A.O., Lin, M., Moore, T., 2018. Scientific assessment of background ozone over the U.S.: implications for air quality management. Elem. Sci. Anth 6 (1), 56. https://doi.org/10.1525/elementa.309.
Janssens-Maenhout, G., et al., 2015. HTAP_v2.2: a mosaic of regional and global emission grid maps for 2008 and 2010 to study hemispheric transport of air pollution. Atmos. Chem. Phys. 15 (19), 11411–11432. https://doi.org/10.5194/acp-15-11411-2015.
Jerrett, M., Burnett, R.T., Pope, C.A., Ito, K., Thurston, G., Krewski, D., Shi, Y., Calle, E., Thun, M., 2009. Long-term ozone exposure and mortality. N. Engl. J. Med. 360 (11), 1085–1095. https://doi.org/10.1056/NEJMoa0803894.
Jiang, Z., et al., 2018. Unexpected slowdown of US pollutant emission reduction in the past decade. Proc. Natl. Acad. Sci. Unit. States Am. 115 (20), 5099–5104. https://doi.org/10.1073/pnas.1801191115.
Krotkov, N.A., Lamsal, L.N., Celarier, E.A., Swartz, W.H., Marchenko, S.V., Bucsela, E.J., Chan, K.L., Wenig, M., Zara, M., 2017. The version 3 OMI NO_2 standard product. Atmos. Meas. Tech. 10 (9), 3133–3149. https://doi.org/10.5194/amt-10-3133-2017.
Lapina, K., Henze, D.K., Milford, J.B., Cuvelier, C., Seltzer, M., 2015. Implications of RCP emissions for future changes in vegetative exposure to ozone in the western U.S,. Geophys. Res. Lett. 42 (10), 4190–4198. https://doi.org/10.1002/2015GL063529.
Lapina, K., Henze, D.K., Milford, J.B., Huang, M., Lin, M., Fiore, A.M., Carmichael, G., Pfister, G.G., Bowman, K., 2014. Assessment of source contributions to seasonal vegetative exposure to ozone in the U.S. J. Geophys. Res. Atmos. 119 (1), 324–340. https://doi.org/10.1002/2013JD020905.
Lin, J.C., Gerbig, C., Wofsy, S.C., Andrews, A.E., Daube, B.C., Davis, K.J., Grainger, C.A., 2003. A near-field tool for simulating the upstream influence of atmospheric observations: the Stochastic Time-Inverted Lagrangian Transport (STILT) model. J. Geophys. Res. Atmos. 108 (D16) https://doi.org/10.1029/2002JD003161.
Malig, B.J., Pearson, D.L., Chang, Y.B., Broadwin, R., Basu, R., Green, R.S., Ostro, B., 2016. A time-stratified case-crossover study of ambient ozone exposure and emergency department visits for specific respiratory diagnoses in California (2005-2008). Environ. Health Perspect. 124 (6), 745–753. https://doi.org/10.1289/ehp.1409495.
Malley, C.S., Henze, D.K., Kuylenstierna, J.C.I., Vallack, H.W., Davila, Y., Anenberg, S.C., Turner, M.C., Ashmore, M.R., 2017. Updated global estimates of respiratory mortality in adults $\geq$ 30 years of age attributable to long-term ozone exposure. Environ. Health Perspect. 125 (8), 087021 https://doi.org/10.1289/EHP1390.
Marchuk, G.I., 1995. Adjoint Equations and Analysis of Complex Systems. Kluwer Academic Publishers, Dordrecht.
Marchuk, G.I., Agoshkov, V.I., Shutyaev, V.P., 1996. Adjoint Equations and Perturbation Algorithms in Nonlinear Problems. CRC Press, New York.
Martin, R.V., Jacob, D.J., Yantosca, R.M., Chin, M., Ginoux, P., 2003. Global and regional decreases in tropospheric oxidants from photochemical effects of aerosols. J. Geophys. Res. Atmos. 108 (D3) https://doi.org/10.1029/2002JD002622.
Medina-Ramón, M., Zanobetti, A., Cavanagh, D.P., Schwartz, J., 2006. Extreme temperatures and mortality: assessing effect modification by personal characteristics and specific cause of death in a multi-city case-only analysis. Environ. Health Perspect. 114 (9), 1331–1336. https://doi.org/10.1289/ehp.9074.
Millet, D.B., Jacob, D.J., Boersma, K.F., Fu, T.-M., Kurosu, T.P., Chance, K., Heald, C.L., Guenther, A., 2008. Spatial distribution of isoprene emissions from North America derived from formaldehyde column measurements by the OMI satellite sensor. J. Geophys. Res. Atmos. 113 (D2) https://doi.org/10.1029/2007JD008950.
Misztal, P.K., Karl, T., Weber, R., Jonsson, H.H., Guenther, A.B., Goldstein, A.H., 2014. Airborne flux measurements of biogenic isoprene over California. Atmos. Chem. Phys. 14, 10631–10647. https://doi.org/10.5194/acp-14-10631-2014.
Palmer, P.I., et al., 2006. Quantifying the seasonal and interannual variability of North American isoprene emissions using satellite observations of the formaldehyde column. J. Geophys. Res. Atmos. 111 (D12) https://doi.org/10.1029/2005JD006689.
Palmer, P.I., Jacob, D.J., Fiore, A.M., Martin, R.V., Chance, K., Kurosu, T.P., 2003. Mapping isoprene emissions over North America using formaldehyde column observations from space. J. Geophys. Res. Atmos. 108 (D6) https://doi.org/10.1029/2002JD002153.
Park, R.J., Jacob, D.J., Field, B.D., Yantosca, R.M., Chin, M., 2004. Natural and transboundary pollution influences on sulfate-nitrate-ammonium aerosols in the United States: implications for policy. J. Geophys. Res. Atmos. 109 (D15), D15204 https://doi.org/10.1029/2003JD004473.
Park, R.J., Jacob, D.J., Kumar, N., Yantosca, R.M., 2006. Regional visibility statistics in the United States: natural and transboundary pollution influences, and implications for the Regional Haze Rule. Atmos. Environ. 40, 5405–5423. https://doi.org/10.1016/j.atmosenv.2006.04.059.
Qu, Z., Henze, D.K., Capps, S.L., Wang, Y., Xu, X., Wang, J., Keller, M., 2017. Monthly top-down NO_x emissions for China (2005–2012): a hybrid inversion method and trend analysis. J. Geophys. Res. Atmos. 122 (8), 4600–4625. https://doi.org/10.1002/2016JD025852.
Qu, Z., Henze, D.K., Cooper, O.R., Neu, J.L., 2020. Impacts of global NOx inversion on NO2 and ozoen simulations. Atmos. Chem. Phys. 20, 13109–13130. https://doi.org/10.5194/acp-20-13109-2020.
Rolph, G., Stein, A., Stunder, B., 2017. Real-time environmental applications and display system: READY, *Environ*. Model. Softw. 95, 210–228. https://doi.org/10.1016/j.envsoft.2017.06.025.
Russell, A.R., Perring, A.E., Valin, L.C., Bucsela, E.J., Browne, E.C., Wooldridge, P.J., Cohen, R.C., 2011. A high spatial resolution retrieval of NO_2 column densities from OMI: method and evaluation. Atmos. Chem. Phys. 11 (16), 8543–8554. https://doi.org/10.5194/acp-11-8543-2011.
Ryoo, J.-M., Johnson, M.S., Iraci, L.T., Yates, E.L., Gore, W., 2017. Investigating sources of ozone over California using AJAX airborne measurements and models: assessing the contribution from long-range transport. Atmos. Environ. 155, 53–67.
Sandu, A., Daescu, D.N., Carmichael, G.R., Chai, T., 2005. Adjoint sensitivity analysis of regional air quality models. J. Comput. Phys. 204 (1), 222–252.
Schnell, R.C., Oltmans, S.J., Neely, R.R., Endres, M.S., Molenar, J.V., White, A.B., 2009. Rapid photochemical production of ozone at high concentrations in a rural site during winter. Nat. Geosci. 2, 120–122. https://doi.org/10.1038/ngeo415.
Schnell, R.C., et al., 2016. Quantifying wintertime boundary layer ozone production from frequent profile measurements in the Uinta Basin, UT, oil and gas region. J. Geophys. Res. Atmos. 121 (11) https://doi.org/10.1002/2016JD025130, 038–11,054.
Shen, L., Jacob, D.J., Zhu, L., Zhang, Q., Zheng, B., Sulprizio, M.P., Li, K., De Smedt, I., González Abad, G., Cao, H., Fu, T.-M., Liao, H., 2019. The 2005–2016 trends of formaldehyde columns over China observed by satellites: increasing anthropogenic emissions of volatile organic compounds and decreasing agricultural fire emissions. Geophys. Res. Lett. 46, 4468–4475 doi:0.1029/2019GL082172, 2019.
Silvern, R.F., Jacob, D.J., Mickley, L.J., Sulprizio, M.P., Travis, K.R., Marais, E.A., Cohen, R.C., Laughner, J.L., Choi, S., Joiner, J., Lamsal, L.N., 2019. Using satellite observations of tropospheric NO_2 columns to infer long-term trends in US NO_x emissions: the importance of accounting for the free tropospheric NO_2 background. Atmos. Chem. Phys. 19, 8863–8878.
Stathopoulou, E., Mihalakakou, G., Santamouris, M., Bagiorgas, H.S., 2008. On the impact of temperature on tropospheric ozone concentration levels in urban environments. J. Earth Syst. Sci. 117 (3), 227–236. https://doi.org/10.1007/s12040-008-0027-9.
Stauffer, R.M., Thompson, A.M., Martins, D.K., Clark, R.D., Goldberg, D.L., Loughner, C.P., Delgado, R., Dickerson, R.R., Stehr, J.W., Tzortziou, M.A., 2015. Bay

breeze influence on surface ozone at Edgewood, MD during July 2011. J. Atmos. Chem. 72, 335–353. https://doi.org/10.1007/s10874-012-9241-6.
Stavrakou, T., Müller, J.-F., De Smedt, I., van Roozendael, M., R, G., van der Werf, Giglio, L., Guenther, A., 2009. Global emissions of non-methane hydrocarbons deduced from SCIAMACHY formaldehyde columns through 2003-2006. Atmos. Chem. Phys. 9, 3663–3679. https://doi.org/10.5194/acp-9-3663-2009.
Verstraeten, W.W., Neu, J.L., Williams, J.E., Bowman, K.W., Worden, J.R., Boersma, K.F., 2015. Rapid increases in tropospheric ozone production and export from China. Nat. Geosci. 8 (9), 690–695. https://doi.org/10.1038/ngeo2493.
Vukovich, F.M., Sherwell, J., 2003. An examination of the relationship between certain meteorological parameters and surface ozone variations in the Baltimore–Washington corridor, *Atmos.* Environ. Times 37 (7), 971–981. https://doi.org/10.1016/S1352-2310(02)00994-9.
Walker, T.W., et al., 2012. Impacts of midlatitude precursor emissions and local photochemistry on ozone abundances in the Arctic. J. Geophys. Res. Atmos. 117 (D1) https://doi.org/10.1029/2011JD016370.
Wise, E.K., 2009. Climate-based sensitivity of air quality to climate change scenarios for the southwestern United States. Int. J. Climatol. 29 (1), 87–97. https://doi.org/10.1002/joc.1713.
Zanobetti, A., Schwartz, J., 2006. Air pollution and emergency admissions in Boston, MA. J. Epidemiol. Community Health 60 (10), 890–895. https://doi.org/10.1136/jech.2005.039834.
Zanobetti, A., Schwartz, J., 2011. Ozone and survival in four cohorts with potentially predisposing diseases. Am. J. Respir. Crit. Care Med. 184 (7), 836–841. https://doi.org/10.1164/rccm.201102-0227OC.
Zhang, L., et al., 2008. Transpacific transport of ozone pollution and the effect of recent Asian emission increases on air quality in North America: an integrated analysis using satellite, aircraft, ozonesonde, and surface observations. Atmos. Chem. Phys. 8 (20), 6117–6136.
Zhang, L., Jacob, D.J., Kopacz, M., Henze, D.K., Singh, K., Jaffe, D.A., 2009. Intercontinental source attribution of ozone pollution at western U.S. sites using an adjoint method. Geophys. Res. Lett. 36 (11) https://doi.org/10.1029/2009GL037950.
Zhang, L., Jacob, D.J., Yue, X., Downey, N.V., Wood, D.A., Blewitt, D., 2014. Sources contributing to background surface ozone in the US Intermountain West. Atmos. Chem. Phys. 14 (11), 5295–5309. https://doi.org/10.5194/acp-14-5295-2014.
Zhang, L., Liu, L., Zhao, Y., Gong, S., Zhang, X., Henze, D.K., Capps, S.L., Fu, T.-M., Zhang, Q., Wang, Y., 2015. Source attribution of particulate matter pollution over North China with the adjoint method. Environ. Res. Lett. 10 (8), 084011 https://doi.org/10.1088/1748-9326/10/8/084011.
Zhu, L., Mickley, L.J., Jacob, D.J., Marais, E.A., Sheng, J., Hu, L., Abad, G.G., Chance, K., 2017. Long-term (2005–2014) trends in formaldehyde (HCHO) columns across North America as seen by the OMI satellite instrument: evidence of changing emissions of volatile organic compounds. Geophys. Res. Lett. 44 (13), 7079–7086. https://doi.org/10.1002/2017GL073859.